ACS APPLIED MATERIALS & INTERFACES

RESEARCH ARTICLE

www.acsami.org

Toughening of Epoxy Matrices with Reduced Single-Walled Carbon Nanotubes

Yadienka Martinez-Rubi,[†] Behnam Ashrafi,[‡] Jingwen Guan,[†] Christopher Kingston,[†] Andrew Johnston,[‡] Benoit Simard,[*,†] Vahid Mirjalili,[§] Pascal Hubert,[§] Libo Deng,[⊥] and Robert J. Young[⊥]

[†]Steacie Institute for Molecular Sciences and [‡]Institute for Aerospace Research National Research Council Canada, Ottawa, K1A 0R6

[§]Department of Mechanical Engineering, McGill University, 817 Sherbrooke Street West, Montréal, QC, H3A 2K6, Canada

[⊥]Materials Science Centre, School of Materials, University of Manchester, Manchester, M13 9PL, United Kingdom

Supporting Information

ABSTRACT:

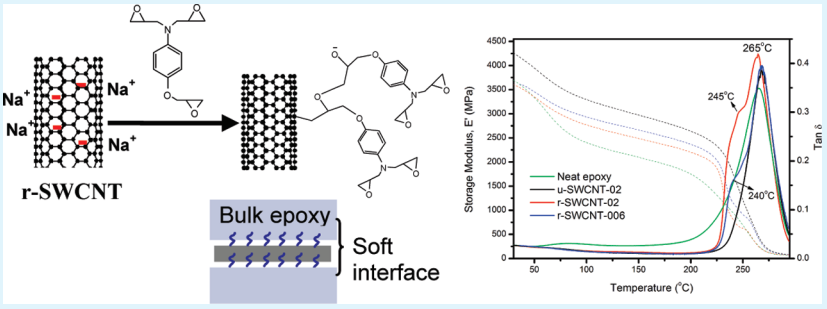

Reduced single-walled carbon nanotubes (r-SWCNT) are shown to react readily at room temperature under inert atmosphere conditions with epoxide moieties, such as those in triglycidyl *p*-amino phenol (TGAP), to produce a soft covalently bonded interface around the SWCNT. The soft interface is compatible with the SWCNT-free cross-linked cured matrix and acts as a toughener for the composite. Incorporation of 0.2 wt % r-SWCNT enhances the ultimate tensile strength, toughness and fracture toughness by 32, 118, and 40%, respectively, without change in modulus. A toughening rate (dK_{IC}/dwt_f) of 200 MPa $m^{0.5}$ is obtained. The toughening mechanism is elucidated through dynamic mechanical analyses, Raman spectroscopy and imaging, and stress−strain curve analyses. The method is scalable and applicable to epoxy resins and systems used commercially.

KEYWORDS: reduced SWCNT, epoxy, composite, toughness

1. INTRODUCTION

The one-dimensional structure; low density; high aspect ratio; and extraordinary mechanical, electrical, and thermal properties of single-walled carbon nanotubes (SWCNT) make them particularly attractive as reinforcing fillers in multifunctional composite materials. Because of their high crystallinity, high aromaticity, and strong van der Waals interactions, pristine SWCNT tend to have smooth defect-free surfaces and exist as ropes or bundles. This leads to poor dispersion/exfoliation and poor interface compatibility with matrices. Hence, a great ongoing challenge in the field of SWCNT/polymer composites is the efficient transfer of nanotube properties into the polymer matrix. Surface functionalization can solve this problem by allowing better dispersion and improved affinity with the matrix.

Carbon nanotubes (CNT) have been incorporated into a wide range of matrices including thermoplastics, thermosets[1,2] and inorganic matrices.[3] CNT/thermoset composites were some of the first to be studied[4] and since then, a range of different functionalization and processing strategies have been used to enhance the physical properties of the matrices. These studies include the investigation of physical blending methods,[5,6] and chemical functionalization.[7−9] It is now well-established that chemical functionalization of CNT is key to effective reinforcement of matrices[1,10] It has also been established that reinforcement is more effective for ductile matrices, such as thermoplastics, than for brittle polymers like thermosets. For example, SWCNT can improve the Young's modulus of thermoplastics by up to 300%,[11] whereas reinforcement of epoxy matrices has not exceeded 100%, with typical results near 35−50%.[1,10] A significant improvement in fracture toughness (K_{IC}) of CNT modified epoxy matrices has been shown for the bidentate epoxy resin diglycidyl ether of bisphenol A with a ratio of fracture toughness improvement versus SWCNT weight fraction (dK_{IC}/dwt_f) of 228 MPa $m^{0.5}$.[12] Additionaly, epoxy matrices with graphene additives have shown a 70% improvement in K_{IC} for a toughening rate, dK_{IC}/dwt_f, of 576 MPa $m^{0.5}$.[13]

Matrix toughness is a key parameter in determining the performance of fiber-reinforced composites. This is particularly

Received: February 22, 2011
Accepted: May 25, 2011
Published: May 25, 2011

true in high performance composites such as those used in aerospace applications where multifunctional thermosetting resins systems with high modulus and high thermal stability but with high brittleness are often used. Here we show that the integration of reduced SWCNT (r-SWCNT) into such brittle epoxy matrices can increase the matrix fracture toughness by 40% at loadings as low as 0.2 wt % with an overall toughening rate value, dK_{IC}/dwt_f, of 200 MPa $m^{0.5}$ without compromising elastic or storage moduli. Owing to electrostatic repulsions and enhanced nucleophilicity, the r-SWCNT readily exfoliate and react directly with glycidyl moieties at room temperature. The mechanical and interfacial properties of these epoxy/SWCNT composites were measured and analyzed.

2. EXPERIMENTAL SECTION

Materials. Most of the focus on epoxy/CNT composite systems has been on bidentate resins such as the well-known diglycidyl ether of bisphenol A (DGEBA). However, most aerospace materials and other high-performance application require tridentate or tetradentate epoxies due to their favorable mechanical properties such as high modulus and thermal stability, coupled with low shrinkage on curing. In this study a commercial tridentate epoxy resin used in the aerospace industry, triglycidyl p-aminophenol (TGAP, trade name of Araldite MY0510), was used as the polymeric matrix precursor. TGAP possesses a high cross-linking density which translates into high modulus and strength; however, this also invariably leads to a brittle polymer. In this work, Aradur HT 976, 4,4′-diaminodiphenylsulfone (DDS), was chosen as the curing agent. The epoxy resin and curing agent were used as received without any further purification; their chemical structures are shown in Figure 1.

SWCNT were synthesized by the two-laser method developed at NRC-SIMS as reported previously.[14] The as-produced material was purified using an in-house method based on successive flotation and centrifugation steps that does not introduce additional defects to the SWCNT wall, as determined by multiple characterization techniques, including absorption and Raman spectroscopy, electron microscopy, and thermogravimetry. The concentration of residual catalysts (Ni and Co) in the purified SWCNT was less than 6 wt % based on thermogravimetric analysis. Absorption spectroscopy was used to determine the carbonaceous purity index of the purified SWCNT material to be 0.110 following the method described by Itkis et al.[15]

Reduction and Integration of SWCNT into the Epoxy Resin. The procedure to reduce (negatively charge) and disperse SWCNT was similar to the method originally described by Penicaud et al.[16] and subsequently by Martinez-Rubi et al.[17] All reactions were conducted under nitrogen. In a typical reaction, 100 mg (8.3 mmol) of purified SWCNT (u-SWCNT) was placed in a Schlenk flask and suspended in dry tetrahydrofuran (THF) with the help of an ultrasonic tip for 15 min and then with an ultrasonic bath for 1 h. A sodium naphthalide solution was prepared in a separate Schlenk flask using 100 mg of sodium (4.3 mmol) and 550 mg (4.3 mmol) of naphthalene in 100 mL of THF. After dissolution of the metal the resultant green solution was added to the SWCNT suspension. The green mixture was placed in a sonication bath for one hour and left overnight under magnetic stirring. The suspension was then carefully transferred under nitrogen to a 250 mL flask and centrifuged at 5000 rpm for 30 min, the excess of sodium naphthalide was discarded and the reduced SWCNT (r-SWCNT) resuspended in dry THF, centrifuged again to remove any residual sodium naphthalide, and resuspended in 70 mL of dry THF using a sonication bath for 30 min. The desired amount of epoxy monomer was dried under vacuum at 80 °C. The stable suspension of r-SWCNT in THF was added under nitrogen to the epoxy monomer and mixed by energetic shaking and bath sonication for 30 min. The THF was removed at room temperature by sparging the mixture with nitrogen for 2 h and with air overnight, then dried in a vacuum oven at 80 °C for 2 h.

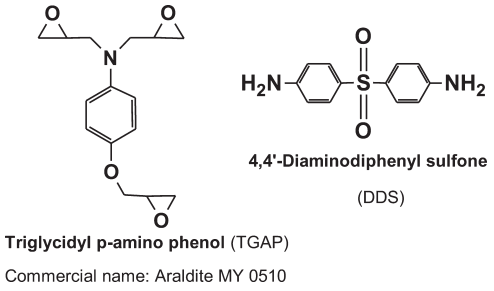

Figure 1. Chemical structures of the epoxy resin used in this study.

Specimen Preparation and Curing Protocol. The curing agent DDS was then added to the epoxy/r-SWCNT mixture in a 100:60 weight ratio which corresponds to a 1:0.9 molar ratio considering an epoxy equivalent weight (EEW) of 92. Specimens at three different loadings, 0.1, 0.2, and 0.3 wt % before adding hardener (0.06, 0.12, and 0.2 wt % after adding it), were prepared using r-SWCNT. The mixtures were mixed manually with a glass road at 80 °C and the temperature was increased to 120 °C at a rate of 1 °C/min while stirring to completely dissolve the DDS particles. Then the samples were degassed for about 40 min at 120 °C until bubbling subsided, then transferred to the corresponding mold where they were cured at 130 °C for 1 h and postcured at 180 °C for 2 h. For comparison purposes, an epoxy sample at 0.2 wt % loading with pristine unfunctionalized SWCNT (u-SWCNT) was also prepared. The pristine SWCNT were incorporated into the epoxy matrix using the same procedure as described above. Samples containing 0.2 wt % of u-SWCNT were named u-SWCNT-02, whereas composites prepared with r-SWCNT at 0.06, 0.1, and 0.2 wt % were named r-SWCNT-006, r-SWCNT-01, and r-SWCNT-02, respectively.

TGA and FTIR Characterization. Solid-state absorption spectroscopy in the mid infrared region (FTIR) was performed using a Varian Digilab FTS 3000MX spectrometer. Thermogravimetric analyses (TGA) were performed on a Netzsch TG 209 F1 Iris. SWCNT used for this analysis were extracted from uncured u-SWCNT/TGAP and r-SWCNT/TGAP mixtures by adding THF and filtering the diluted mixture. The separated SWCNT were washed with more THF, water and acetone. The product was then repeatedly suspended in THF and acetone using an ultrasonic bath. The suspensions were centrifuged and finally filtered to recover the product which was washed with acetone and dried under a vacuum at 100 °C.

Raman Spectroscopy. Raman spectra were recorded on a Renishaw inVia micro-Raman spectrometer. Samples of free-standing SWCNT were measured on a glass slide using a 514, 633, or 785 nm laser focused to approximately 1 μm through a 50x objective. Laser power density at the sample was maintained below 3 kW/cm^2 to avoid laser-induced heating effects. For Raman mapping the top surface of 0.5 mm thick SWCNT-epoxy samples were successively polished using 600, 800, and 1200 grit grinding paper. Next, appropriate polishing pads and lubricants were used to polish the samples with 3 and 1 μm diamond abrasive liquids to obtain a smooth surface. Mapping of the SWCNT concentration distribution and G′-band peak position was done using a spectral imaging mode. Raman images were acquired for 60 μm × 90 μm regions at 1 μm intervals in x and y using a 50× objective and an excitation wavelength of 785 nm. Raman spectra were also obtained during the deformation of specimen beams during mechanical loading using a Renishaw micro-Raman spectrometer with a 633 nm laser. The strain in the specimen was measured using a strain gage and the laser beam was always polarized parallel to the axis of tensile strain.

Scheme 1. Formation of Reduced SWCNT and Their Reaction with the Epoxy Monomer TGAP

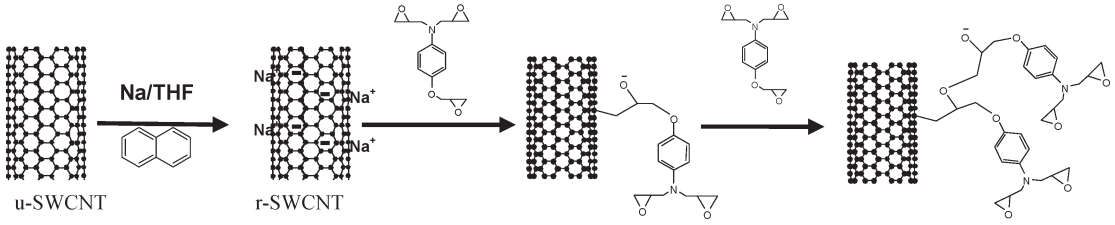

Tensile Measurements. Testing was performed on an MTS 858 Table Top Servohydraulic test frame equipped with hydraulic grips. Each dog-bone coupon was placed in the grips and tested in displacement control to failure at a loading rate of 1.27 mm/min. The strain at peak load or elongation (ε_{max}) and ultimate tensile stress (UTS) were determined for each specimen. Young's modulus (E) was obtained from the slope of the linear fit of the initial linear section of the stress−strain curve. Finally, the toughness (G) was estimated by calculating the area under the curve using eq 1

$$G = \sum_{\varepsilon=0}^{\varepsilon_{max}} \sigma \Delta \varepsilon \qquad (1)$$

Fracture Toughness Measurements. Specimens for fracture toughness tests were prepared according to the standard test method for measurement of fracture toughness of polymer materials, ASTM D 5045-91. Of the two methods covered by the standard, the Single Edge Notch Bending test was used with sample dimensions chosen to be 20 mm × 4 mm × 2 mm to minimize the use of material. The notch depth was 2 mm with a span of 16 mm. A mold was designed to produce 10 fracture toughness test samples at a time.

Dynamic Mechanical Thermal Analysis (DMA). DMA analysis was performed using a Q800-TA Instruments dynamic mechanical analyzer. Tests were done by the force control module using a 3-point bending fixture. Tests were performed at a frequency of 1 Hz with a temperature sweep from room temperature to 300 °C at a ramp rate of 3 °C/min. DMA coupons were about 60 mm long, 4 mm wide, and 3.5 mm thick, and a total of 3 tests were performed for each batch of material.

3. RESULTS AND DISCUSSION

SWCNT can be exfoliated in standard solvents by reduction with an alkali metal through electron transfer mediated by alkali-naphthalene-tetrahydrofuran complexes.[16] As the SWCNT charge negatively, they exfoliate due to electrostatic repulsion and form stable suspensions in polar solvents. In addition, r-SWCNT exhibit higher reactivity than neutral SWCNT toward various reagents.[17] Because their nucleophilic character is increased, r-SWCNT can react readily at room temperature with the epoxide groups of epoxy resins through ring-opening nucleophilic addition to create a direct connection between the resin and the nanotubes. The reaction propagates (Scheme 1) until the alkoxide is neutralized, usually though hydrolysis. This reaction ensures excellent interface compatibility and maintains the stability of the dispersion once the solvent is removed and the alkoxide moieties have hydrolyzed.

The r-SWCNT/THF suspension was integrated into the epoxy resin under nitrogen flow because of the air sensitivity of r-SWCNT. It is worth noting that when the solvent is removed via nitrogen and the r-SWCNT/epoxy mixture is maintained under nitrogen for a few days, the viscosity of the mixture gradually increases, forming first a rubbery and subsequently a solid material indicative of a cured system. This is because, as illustrated in Scheme 1, of the propagation of the ring-opening reaction through the alkoxide groups. For this work, once the solvent is removed the r-SWCNT/epoxy mixture is exposed to air to quench the propagation reaction. Once the sample is exposed to air, no further change in viscosity is observed for several months.

To further evaluate the reaction between r-SWCNT and TGAP, SWCNT extracted from uncured r-SWCNT/TGAP and u-SWCNT/TGAP mixtures were characterized by TGA and FTIR. After carefully washing the extracted SWCNT, TGA showed a weight loss of 12% and 27% for u-SWCNT and r-SWCNT, respectively, while only a 2% weight loss was observed for purified SWCNT (Figure 2 left). The 12% weight loss of u-SWCNT indicates the presence of physically adsorbed TGAP monomers even after carefully washing the sample. On the other hand, the weight loss observed for r-SWCNT is twice as large, suggesting the grafting of TGAP oligomers on the SWCNT. Additionally, FTIR spectra showed important differences between the three samples (Figure 2 right). Purified SWCNT do not show any significant feature, whereas very weak bands are observed for u-SWCNT; specifically, a peak at 1510 cm^{-1} can be assigned to TGAP aromatic rings adsorbed onto the SWCNT, in agreement with TGA results. The FTIR spectrum of r-SWCNT clearly shows different features which can be assigned to the attached functional groups. A significant feature is the broad band centered at 3440 cm^{-1}, which corresponds to the stretching of −OH groups originated in the homopolimerization reaction.[18] The band doublet at 2919/2856 cm^{-1} standing for CH_2 vibration modes is clearly visible, whereas the band at 1721 cm^{-1} indicates the C═O stretching mode of aldehyde groups derived by isomerization of epoxide groups.[19] The bands at 1658, 1593, and 1510 cm^{-1} correspond to aromatic rings and the out-of-plane 1:4 ring substitution vibration mode is visible at 822 cm^{-1}. The peaks at 1237 and 1105 cm^{-1} infer the presence of C−O bonds.[19]

Dispersion and Interface Characterization. The dispersion of the uncured SWCNT/epoxy composites after the addition of the curing agent was analyzed with an optical microscope while heating the sample to simulate the curing process. Figure 3 displays optical images of these composites taken at different temperatures. The top row of images corresponds to r-SWCNT-02 composites, where the curing agent DDS was mixed at room temperature; the middle and bottom ones correspond to u-SWCNT-02 and r-SWCNT-02, respectively, where the DDS was mixed at 100 °C and then deposited onto the sample holder for analysis.

As can be observed in Figure 3A, DDS particles (identified by circles) are not dissolved into the epoxy at room temperature. As the temperature is increased the solid gradually began to dissolve (Figures 3B and 3C) displacing the nanotubes and leaving transparent areas (identified by arrows) where no nanotubes are present, leading to a composite with an inhomogeneous

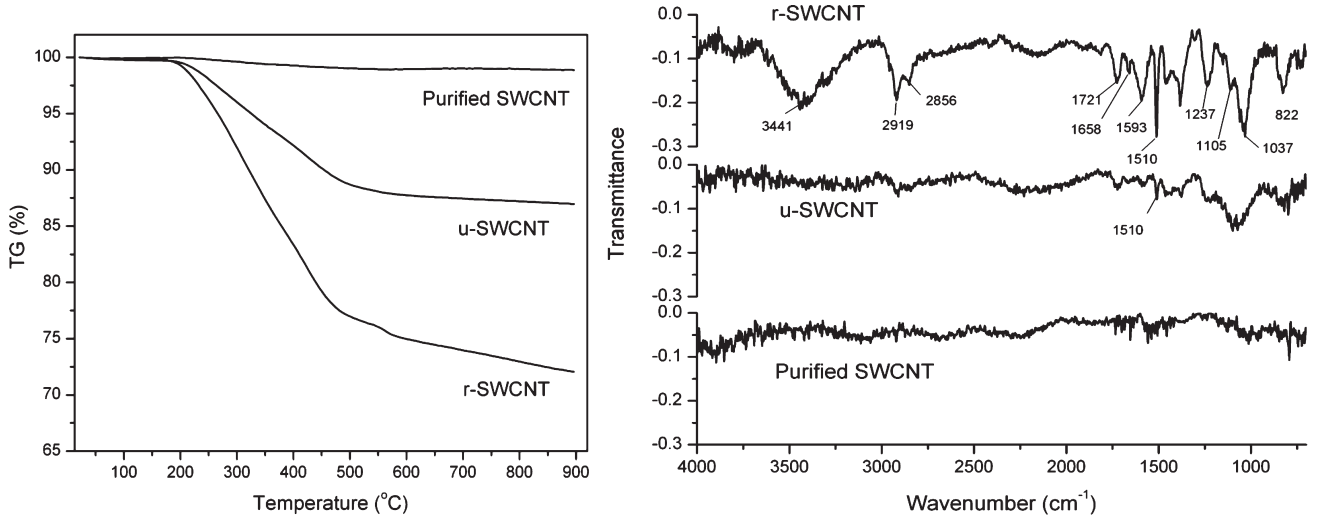

Figure 2. TGA results (left) and FTIR (right) spectra of purified SWCNT and SWCNT extracted from r-SWCNT/TGAP and u-SWCNT/TGAP mixtures.

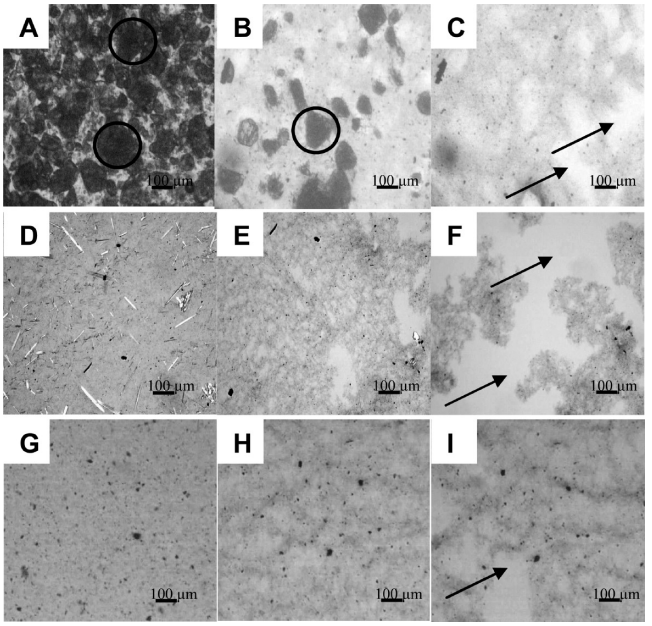

Figure 3. Optical images of the uncured SWCNT/epoxy composites at different temperatures; (A, D, G) at 30 °C; (B, E, H) at 90 °C; and (C, F, I) at 130 °C. The top and bottom rows of images correspond to r-SWCNT-02 composites and the middle row to u-SWCNT-02.

distribution of the reinforcement. On the other hand, Figures 3D and 3G show optical images of u-SWCNT-02 and r-SWCNT-02 where the DDS was dissolved at 100 °C prior to analyzing the samples. In the case of u-SWCNT-02, although the distribution of nanotubes was homogeneous at room temperature (Figure 3D), local clustering of the nanotubes occurred when the temperature was gradually increased (Figures 3E and 3F). This behavior has been observed by other authors and it has been attributed to some extent to changes in viscosity, leading to an increase of the diffusion coefficient and to the increased kinetic energy of the particles at higher temperature.[20] On the other hand, optical images taken at different temperatures of r-SWCNT-02 where DDS was dissolved before doing the analysis (Figure 3G, H, I) showed less reagglomeration and hence more homogeneous dispersion even at higher temperatures. This result indicates that the introduction of reduced SWCNT and their covalent attachment to the epoxy monomer helps to increase the repulsive barrier between nanotubes and maintain the stability of the dispersion, but that the processing conditions also have to be controlled. On the basis of these results, for specimen preparation, after the addition of the curing agent, the sample was mixed at 100 °C until the DDS was completely dissolved and mixed at 10 min intervals while degassing at 120 °C in order to maintain SWCNT dispersion and avoid the formation of local clustering. At this temperature, as the cross-linking reaction begins, the formation of higher molecular weight species increases the system viscosity and restricts Brownian motion enough to stabilize the nanotube dispersion against agglomeration without affecting processability.

Raman spectroscopy is one of the most extensively employed methods for the characterization of carbon nanotubes, particularly when trying to demonstrate covalent functionalization to the SWCNT wall.[21] The most characteristic features of the Raman spectrum of SWCNT are the diameter-dependent radial breading mode (RBM) in the 150−250 cm^{-1} region, the tangential, Graphitic (sp^2 character) modes or G band, near 1600 cm^{-1}, the dispersive disorder-induced D-band around 1300 cm^{-1} and the second-order G′-band around 2600 cm^{-1}. When addends are covalently anchored to the sidewall, the hybridization of the C atoms changes from sp^2 to sp^3 which yields a commensurate intensity increase in the D-band. Figure 4 shows the Raman spectra of purified SWCNT and SWCNT/epoxy composites taken with two different excitation lasers. Figure 4A compares the 514 nm Raman spectra of purified pristine SWCNT together with cured r-SWCNT-02 composites. For the case of the r-SWCNT-02 composite, the SWCNT Raman signal is superposed on a strong fluorescence background from the polymer matrix. However, this can be overcome by using 785 nm excitation, as can be observed in Figure 4B.

The spectrum of the r-SWCNT-02 composite was compared to the spectra of free-standing purified SWCNT (u-SWCNT) and u-SWCNT-02 (that is u-SWCNT added to the resin) composites, but no significant change in the D to G band intensity ratio (I_D/I_G) was observed. The 514 and 785 nm excitation lasers probe primarily semiconducting SWCNT in our samples due to

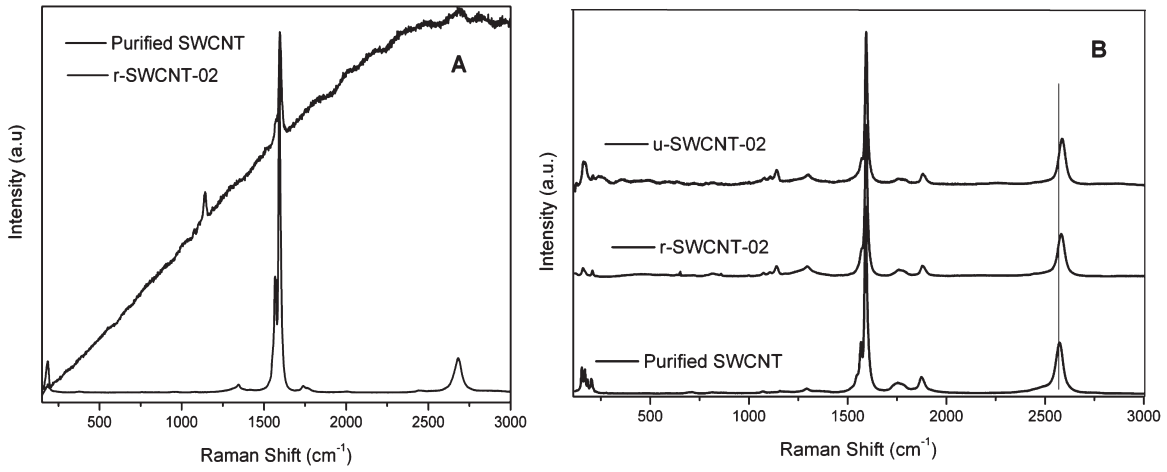

Figure 4. Raman spectra of (A) purified SWCNT and SWCNT/epoxy composites using a 514 nm excitation laser line and (B) a 785 nm excitation laser line.

the resonant nature of Raman scattering in SWCNT; similar results were obtained using a 633 nm laser (not shown) which probes mainly metallic nanotubes in our samples. These results indicate that the degree of functionalization is too low to be detected by Raman and/or that the covalent anchoring and initiation of the propagation reaction occurs on existing defects or at the tip ends of the SWCNT such that no increased disorder is introduced into the nanotube framework. Raman spectroscopy has also been used to investigate the local strains in CNT/epoxy composites.[22−24] As can be observed in Figure 4B, the G′-band of SWCNT embedded in r-SWCNT-02 and u-SWCNT-02 composites upshift by 7 and 14 cm^{-1}, respectively, compared to free-standing SWCNT (2573 cm^{-1}). Panels C and D of Figure 5 show representative 2-D Raman spectral images of the G′-band position for a 60 × 90 μm^2 area of u-SWCNT-02 and r-SWCNT-02 composites. Clearly these results confirm that the nanotubes in u-SWCNT-02 are at higher strain than in r-SWCNT-02 composites and that the strain distribution is not homogeneous. This upward shift of the vibrational frequency has been interpreted as a compression of the C−C bond due to residual stress build-up as temperature is lowered, due to the thermal shrinkage and the differences in the coefficients of thermal expansion between the polymer matrix and the SWCNT. The magnitude of this residual stress has been found to increase with increasing difference between T_g and room temperature.[25] Recently, it has been shown that the magnitude of compressive strain experienced by SWCNT can be used as a good indicator of improvement in coupling strength of SWCNT to the matrix.[24] According to this observation, the SWCNT in both of our samples are loaded under compression stress at room temperature; however, the coupling strength is lower in composites made with reduced SWCNT. Large residual stress in composite materials may lead to the formation of cracks and reduction of strength.[25] On the other hand, it has been reported that it can also have a positive influence on the toughness of the composites.[26]

Additionally, Raman intensity maps were used to quantitatively evaluate the 2-dimensional SWCNT dispersion at a 1 μm length scale. The intensities of the Raman modes are proportional to SWCNT concentration within the sampling volume, therefore the G′-band intensity distribution can be used to evaluate the distribution of SWCNT along the composite sample surface. The dispersion was evaluated using a method described by Du et al.[27] in which the Raman intensities for each image are normalized to a mean of 100, and the standard deviation (SD) about that average is calculated. Raman images of the G′-band intensity distribution of 60 × 90 μm regions of u-SWCNT-02 and r-SWCNT-02 samples are shown in panels A and B, respectively, of Figure 5. It can be observed that the 3D contour plot of normalized Raman intensity of r-SWCNT-02 is flatter than that of u-SWCNT-02, with standard deviations of 26 and 38, respectively. This indicates that the nanotubes in r-SWCNT-02 composites are better dispersed in the epoxy matrix than in u-SWCNT-02 composites, as expected from the natural exfoliation of r-SWCNT. Cross-sectional SEM images of samples fractured under tensile load were used to evaluate the dispersion on a scale below 1 μm (see the Supporting Information, Figure S1). A few 23 nm bundles were observed in u-SWCNT-02 composites, whereas in r-SWCNT-02, smaller bundles (11 nm) were visible together with 35−46 nm fibrils.[12] Similar fibril structure has been observed in a bisphenol A-based epoxy reinforced with amido-amine-functionalized multiwalled carbon nanotubes exhibiting crazing.[12]

The G′-band in the Raman spectrum has also been used to study SWCNT-matrix stress transfer using the method developed by Young et al.[28,29] A linear downshift of this peak as a function of applied tensile strain has been observed and has been used to evaluate stress transfer efficiency in composite materials. The results of the strain-dependent Raman spectroscopy measurements for u-SWCNT-02 and r-SWCNT-02 composites are presented in Figure 6. The shift of the Raman peak reveals that load is transferred from the matrix to the SWCNT. However, the steeper slope of the u-SWCNT-02 composite (−17.4 cm^{-1}/%, compared to −10 cm^{-1}/% of the r-SWCNT-02 composite) suggests a more efficient load transfer for composites containing pristine SWCNT. It is possible to use the slopes of the lines in Figure 6 to estimate the effective Young's modulus of the SWCNT.[29] Assuming that the nanotubes are arranged randomly in plane, then the inherent band shift factor for nanotubes aligned parallel to the stressing direction, S_0 is related to the measured line slopes in Figure 6, $S_{VV}(0)$ by the relation

$$S_0 = 1.3S_{VV}(0) \quad (2)$$

This equation takes into account the fact that nanotubes lying in different directions to the applied stress axis also contribute to the

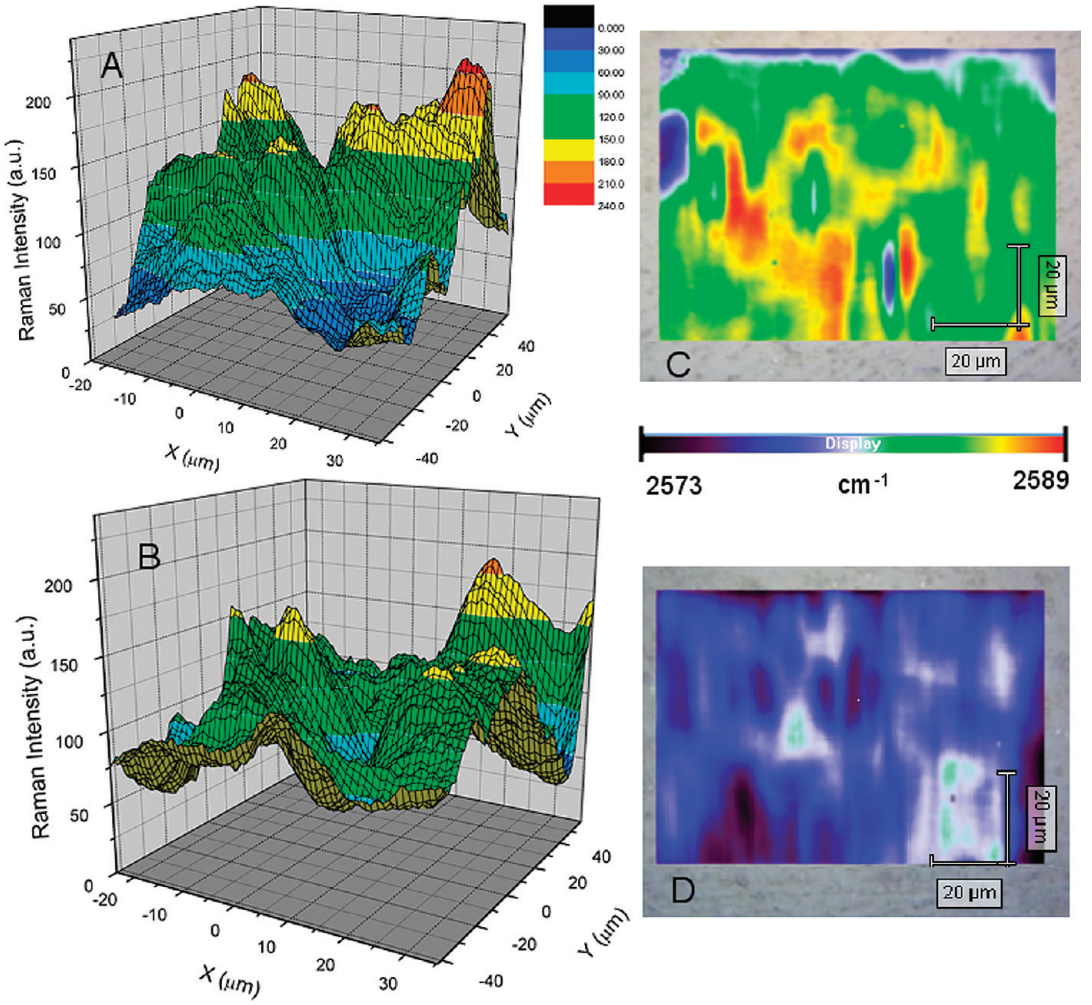

Figure 5. Raman image of u-SWCNT-02 (top) and r-SWCNT-02 (bottom) composites: (A, B) Raman image of the G′-band intensity distribution; (C, D) G′-band peak position. (λ_{exc} 785 nm).

Raman spectrum.[29] The effective modulus of the nanotubes, E_{eff}, can then be determined using the universal calibration[28] through the equation[29]

$$E_{eff} = S_0/-0.05 \quad (3)$$

where E_{eff} is in GPa and S_0 has units of cm^{-1}/% strain. The slopes of the lines in Figure 6 of −17.4 and −10 cm^{-1}/% for the u-SWCNT-02 composite and the r-SWCNT-02 composite lead to effective Young's modulus values of 450 and 260 GPa, respectively, for the nanotubes in the two systems. The mechanical properties of these composites were also studied and will be discussed (vide infra).

Tensile and Fracture Behavior. Tensile tests were performed to determine the mechanical properties of r-SWCNT and u-SWCNT composites and the neat resin in order to evaluate the effectiveness of this functionalization strategy. Figure 7 shows representative stress−strain curves obtained for these materials. Figure 8 summarizes the tensile properties.

The tensile results indicate that the incorporation of pristine unfunctionalized SWCNT into the epoxy resin does not lead to an improvement in any of the measured mechanical properties and even causes some degradation. On the other hand, as can be observed in Figure 8, reduced SWCNT noticeably increase both

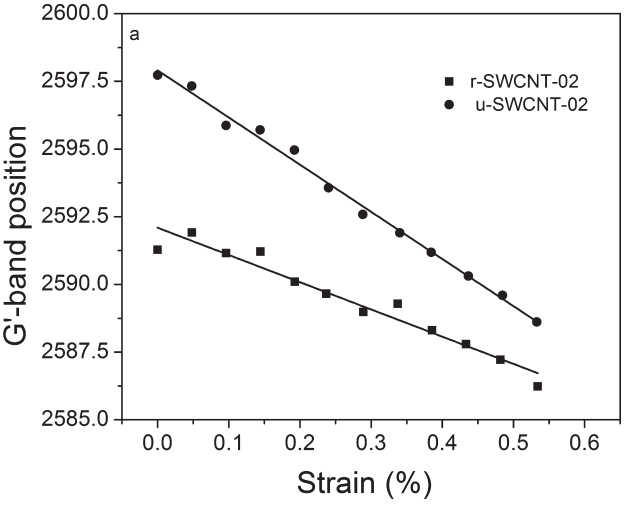

Figure 6. Shift in the G′-band position as a function of composite applied strain for u-SWCNT-02 and r-SWCNT-02 samples.

the ultimate tensile strength and strain. The ultimate tensile strength (UTS), ultimate tensile strain and toughness increase by

32, 52 and 118% respectively by incorporation of 0.2 wt % of reduced SWCNT, whereas no significant changes were observed for the Young's modulus. Since effective Young's modulus of the pristine and reduced SWCNTs is 450 and 260 GPa respectively, then any increase in Young's modulus on adding only 0.2% of these nanotubes to an epoxy resin with a modulus of ~4.1 GPa would be within the experimental error (±0.3 GPa). Because these composites have not shown any significant stiffness enhancement, it is believed that the increased ductility is then most likely due to resin mobility enhancement in the presence of SWCNT. It appears that the improvement in ductility increases with nanotube loading, indicating the involvement of the nanotubes in the reinforcement mechanism. However, the standard deviation is too high to confirm the existence of a trend.

The toughness, defined as the energy absorbed by the material prior to failure, is an important property to improve for thermosetting polymers, especially in the case of this tridentate epoxy resin, which possesses a high strength and modulus as compared to commercial bidentate resins such as the extensively studied diglycidyl ether of bisphenol A. Toughness improvement is a crucial step for application of these resins for development of laminates composites with improved interlaminar properties.[30,31] To further investigate the toughness of these composites, the fracture toughness was also measured and compared with the neat epoxy and u-SWCNT composites. As can be observed in Figure 9, these measurements indicate that the fracture toughness increases with r-SWCNT loading. The K_{IC} value increases from 1.09 ± 0.3 MPa $m^{0.5}$ for the neat epoxy to 1.31 ± 0.28, 1.38 ± 0.14, and 1.51 ± 0.06 MPa $m^{0.5}$ by incorporation of 0.06, 0.12, and 0.2 wt %, respectively, of reduced SWCNT, yielding a toughening rate of (dK_{IC}/dwt) of 200 MPa $m^{0.5}$. It is worth noting that the error bars for the neat epoxy are very high because of the brittleness of this resin. Interestingly, the error bars for the composites decreases with increasing r-SWCNT loading, indicating the effective role of the filler in improving fracture toughness.

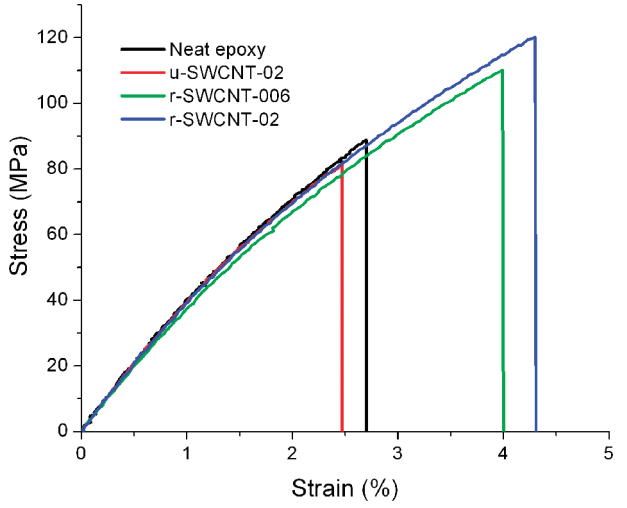

Figure 7. Tensile stress−strain curves of the SWNCT/epoxy samples and neat epoxy resin.

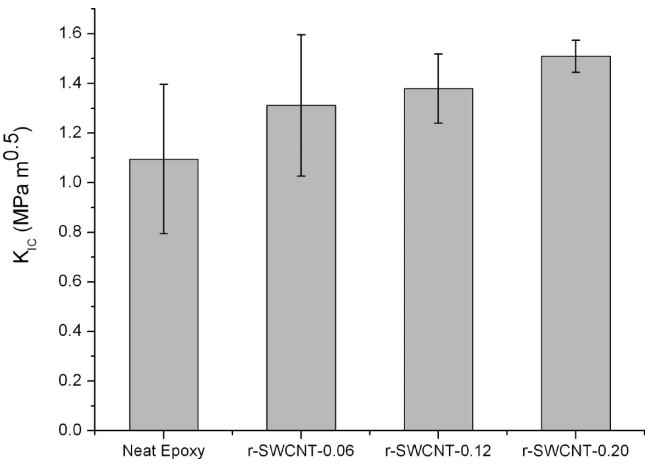

Figure 9. Fracture toughness of r-SWCNT composites at different loadings compared to neat epoxy matrix.

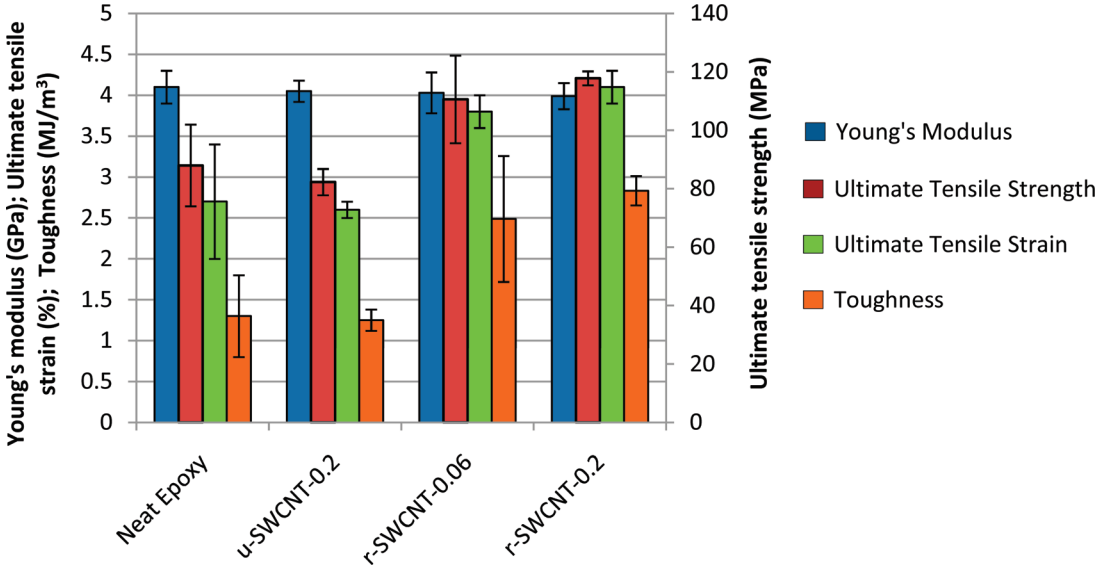

Figure 8. Summary of mechanical properties obtained from tensile tests.

In addition to the improved dispersibility, the improvement in mechanical properties observed with r-SWCNT may be attributed to grafting of epoxy oligomers to the SWCNT wall (Scheme1), which acts as both a dispersing agent and a covalent matrix binding agent. This reaction may change the stoichiometry and microstructure of the network at the matrix/nanotube interface. However, the low degree of covalent connections between the nanotubes and the matrix, as detected by Raman spectroscopy, should not have a significant impact in the overall matrix stoichiometry. The low degree of covalent connections between the nanotubes and the matrix compounded by the low concentration of r-SWCNT could be responsible for low load transfer to the nanotubes leading to no improvement in Young's modulus. On the other hand reduced SWCNT clearly improved the matrix ductility. Similar behavior was observed by Liu et al.[32] when studying the reinforcement by MWCNT in a rubbery and a glassy epoxy resin. Contrary to the results obtained for the rubbery epoxy, no improvement in Young's modulus was observed for the glassy epoxy but a significant (50%) improvement was obtained for the impact toughness. The authors attributed this enhancement to the higher flexibility and deformability under load of the nanotubes compared to micrometer-scale fiber reinforcements. Moreover, it has been reported that CNT take on a more significant reinforcement role in composites with soft matrix than with hard matrix.[33] In our system, the reaction represented in Scheme1 could form a less reticulated, softer structure at the SWCNT/matrix interface, which could increase matrix mobility at the interface.

Dynamic Mechanical Behavior. The literature has generally shown that decreasing the cross-link density causes toughness to increase because of the formation of a looser, more mobile network that is able to absorb energy more efficiently than a highly cross-link network. These structural changes can also modify the glass transition temperature (T_g) and many studies have found that decreasing the cross-link density caused the T_g to decrease. DMA was used to investigate the effect of unfunctionalized and reduced SWCNT on the T_g of the epoxy matrix. In the DMA technique, two different moduli are determined as a function of temperature, an elastic or storage modulus (E'), which is related to the ability of the material to return or store energy, and an imaginary or loss modulus (E''), which relates to the ability of the polymer to disperse energy. The temperature dependence of the ratio E''/E' is called tan δ (tan delta) and the maximum value in a tanδ vs temperature plot is taken as an estimate of the T_g. Dynamic mechanical properties of the neat epoxy, u-SWCNT-02 composite and r-SWCNT composites at two different loadings are shown in Figure 10.

Pure epoxy shows an α-relaxation peak at ∼265 °C that corresponds to the glass transition temperature (solid green line in Figure 10). Interestingly, r-SWCNT-02 and r-SWCNT-006 composites show two relaxation peaks, which indicate the presence of two T_gs. The smaller relaxation peak at ∼245 °C for r-SWCNT-02 and ∼240 °C for r-SWCNT-006 occurs at a temperature that is lower than the T_g of the neat epoxy and its intensity increases with nanotube loading. The larger relaxation peak occurs at 265 °C, which is the same temperature of the α-relaxation peak of the neat epoxy. On the other hand u-SWCNT-02 composites only show a relaxation peak at 265 °C. Observations of two T_g peaks have been reported before for clay/epoxy composites and polyimide/multiwall carbon nanotube composite.[34−36] There are several explanations for this behavior. Velmurugan and Mohan attributed the two relaxation peaks to hard and soft segments in the epoxy and hard segments were ascribed to the segments arrested at the neighborhood of a clay−epoxy interface. Marouf et al. did a detailed analysis of this phenomenon and concluded that the presence of two T_g transitions regions implies different temperature dependences of molecular motions in different length-scales.[35] The lower glass transition suggests the presence of domains that provide easier molecular motions for polymer segments. They also concluded that segment mobility in the interphase region depends on the strength of the interaction between the solid surface and the polymer chains.

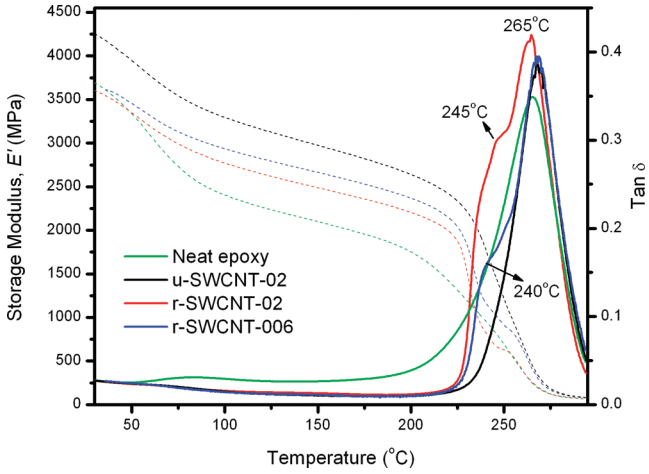

Figure 10. Typical DMA results of the SWCNT/epoxy composites studied; dashed line for the storage modulus and solid lines for the tanδ.

On the basis of the results obtained for our system, we put forward that the observation of the lower T_g in r-SWCNT composites results from the presence of a soft protective coating of self-propagated linkages among epoxy monomers around the SWCNT, which creates a network with lower cross-link density at the interface region while the bulk cross-link density is not significantly affected. The concept of a soft interface has also been demonstrated recently for amido-amine functionalized multiwalled carbon nanotubes in a bidentate epoxy matrix (diglycidyl ether of bisphenol A).[12] In our system, this concept is supported by the observation that only one relaxation peak was present in u-SWCNT composites, whereas in r-SWCNT composites, the intensity of the lower temperature relaxation peak increases with nanotube loading which indicates that the concentration of this lower T_g domain increases with increasing concentration of reduced nanotubes in the resin. Such microstructural changes at the interface also explain the lower strain observed by Raman spectroscopy for nanotubes embedded in r-SWCNT composites compared to u-SWCNT composites. The storage modulus data (E') of the neat resin, u-SWCNT and r-SWCNT composites are also shown in Figure 10 (dashed lines). It can be seen that at room temperature, the E' of composites containing u-SWCNT shows a 15% enhancement, whereas no improvement is observed for r-SWCNT composites. This result is in agreement with the observations made by strain-dependent Raman spectroscopy (Figure 6) where a more efficient load transfer was observed for composites containing pristine SWCNT, which have a higher effective Young's modulus than the reduced SWCNT. These results are in apparent contradiction with tensile results

(Figure 8), in which no statistically significant difference was found between the unfunctionalized SWCNT batch and the neat resin. This discrepancy might be due to different techniques employed to manufacture the test specimens. Whereas DMA coupons were cut from cured bulk specimens, tensile coupons were prepared using an injection molding technique. It is possible that the shear forces involved with the molding reduced the quality of dispersion as compared to the DMA coupons, more specifically for the unfunctionalized SWCNT material. On the other hand, above 100 °C in the glassy state, the storage modulus of the reduced SWCNT composites was found to be higher than the neat epoxy. This indicates that in the glassy state the motion of epoxy matrix chains is restricted by the well-dispersed SWCNT network.

3. CONCLUSIONS

We have presented a scalable and simple method to incorporate SWCNT into epoxy resins. The direct integration of reduced SWCNT were shown to improve the toughness and fracture toughness of a high performance aerospace resin at rates of dG/dwt_f = 674 MJ/m^3 and dK_{IC}/dwt_f = of 200 MPa m$^{0.5}$, respectively, without compromising the modulus and T_g. Raman measurements showed a relatively low degree of covalent anchoring on the side wall of the SWCNT and that, at room temperature, SWCNT embedded in r-SWCNT composites experience a lower compression strain than SWCNT in u-SWCNT composites. In addition, strain-dependent Raman spectroscopy measurements suggest better load transfer efficiency in composites containing pristine SWCNT. In accord with this result, DMA measurement showed 15% improvement in storage modulus for u-SWCNT composites, whereas no improvement was observed for r-SWCNT samples. On the other hand, DMA measurements show two relaxation peaks in r-SWCNT composites, which indicate the presence of two T_g values. The lower-temperature T_g is herein attributed to the formation of a relatively "soft" interface layer of epoxy next to the surface of SWCNT and the higher-temperature T_g to the SWCNT-free higher density resin. The large surface area of well-dispersed SWCNT within r-SWCNT composites results in a significant contribution of this softer interface to the matrix mobility. The observed improvement in toughness makes this functionalization strategy an attractive alternative for the development of laminated composites with improved interlaminar properties.

■ ASSOCIATED CONTENT

Supporting Information. This material is available free of charge via the Internet at http://pubs.acs.org.

■ AUTHOR INFORMATION

Corresponding Author

*E-mail: benoit.simard@nrc-cnrc.gc.ca (B.S.).

■ REFERENCES

(1) Spitalsky, Z.; Tasis, D.; Papagelis, K.; Galiotis, C. *Prog. Polym. Sci.* **2010**, *35*, 357–401.
(2) Coleman, J. N.; Khan, U.; Blau, W. J.; Gun'ko, Y. K. *Carbon* **2006**, *44*, 1624–1652.
(3) Estili, M.; Kawasaki, A.; Sakamoto, H.; Mekuchi, Y.; Kuno, M.; Tsukada, T. *Acta Mater.* **2008**, *56*, 4070–4079.
(4) Ajayan, P. M.; Stephan, O.; Colliex, C.; Trauth, D. *Science* **1994**, *265*, 1212–1214.
(5) Gojny, F. H.; Wichmann, M. H. G.; Köpke, U.; Fiedler, B.; Schulte, K. *Compos. Sci. Technol.* **2004**, *64*, 2363–2371.
(6) Thostenson, E. T.; Chou, T. W. *Carbon* **2006**, *44*, 3022–3029.
(7) Zhu, J.; Kim, J.; Peng, H.; Margrave, J. L.; Khabashesku, V. N.; Barrera, E. V. *Nano Lett.* **2003**, *3*, 1107–1113.
(8) Li, Y. H.; Wang, S.; Luan, Z.; Ding, J.; Xu, C.; Wu, D. *Carbon* **2003**, *41*, 1057–1062.
(9) Tseng, C. H.; Wang, C. C.; Chen, C. Y. *Chem. Mater.* **2007**, *19*, 308–315.
(10) Ma, P. C.; Siddiqui, N. A.; Marom, G.; Kim, J. K. *Compos., Part A* **2010**, *41*, 1345–1367.
(11) Coleman, J. N.; Cadek, M.; Blake, R.; Nicolosi, V.; Ryan, K. P.; Belton, C.; Fonseca, A.; Nagy, J B.; Gun'ko, Y. K.; Blau, W. *Adv. Funct. Mater.* **2004**, *14*, 791–798.
(12) Zhang, W.; Srivastava, I.; Zhu, Y.-F.; Picu, C. R.; Koratkar, N. *Small* **2009**, *5*, 1403–1407.
(13) Rafiee, M. A.; Rafiee, J.; Srivastava, I.; Wang, Z.; Song, H.; Yu, Z.-Z.; Koratkar, N. *Small* **2010**, *6*, 179–183.
(14) Kingston, C. T.; Jakubek, Z. J.; Denommee, S.; Simard, B. *Carbon* **2004**, *42*, 1657–1664.
(15) Itkis, M. E.; Perea, D.; Jung, R.; Niyogi, S.; Haddon, R. C. *J. Am. Chem. Soc.* **2005**, *127*, 3439–3448.
(16) Penicaud, A.; Poulin, P.; Derre, A.; Anglaret, E.; Petit, P. *J. Am. Chem. Soc.* **2005**, *127*, 8–9.
(17) Martínez-Rubí, Y.; Guan, J. W.; Lin, S.; Scriver, C.; Sturgeon, R. E.; Simard, B. *Chem. Commun.* **2007**, *48*, 5146–8.
(18) Morgan, R. J.; Mones, E. T. *J. Appl. Polym. Sci.* **1987**, *33*, 999–1020.
(19) Nakanishi, K.; Solomon, P. H. In *Infrared Absorption Spectroscopy*, 2nd ed.; Holden-Day, Inc.: Oakland, CA, 1997.
(20) Martin, C. A.; Sandler, J. K.W.; Shaffer, M. S. P.; Schwarz, M. K.; Bauhofer, W.; Schulte, K.; Windle, A. H. *Compos. Sci. Technol.* **2004**, *64*, 2309–2316.
(21) Graupner, R. *J. Raman Spectrosc.* **2007**, *38*, 673–683.
(22) Lucas, M.; Young, R. J. *Compos. Sci. Technol.* **2007**, *67*, 840–843.
(23) Lourie, O.; Wagner, H. D. *J. Mater. Res.* **1998**, *13*, 2418–2422.
(24) Hadjiev, V. G.; Warren, G. L.; Sun, L.; Davis, D. C.; Lagoudas, D. C.; Sue, H. J. *Carbon* **2010**, *4* (8), 1750–1756.
(25) Lange, J.; Toll, S.; Månson, J. E.; Hult, A. *Polymer* **1995**, *36*, 3135–3141.
(26) Todd, R. I.; Boccaccini, A. R.; Sinclair, R.; Yallee, R. B.; Young, R. *Acta Mater* **1999**, *47*, 3233–3240.
(27) Du, F.; Scogna, R. C.; Zhou, W.; Brand, S.; Fischer, J. E.; Winey, K. I. *Macromolecules* **2004**, *37*, 9048–9055.
(28) Cooper, C. A.; Young, R. J.; Halsall, M. *Compos., Part A* **2001**, *32*, 401–411.
(29) Deng, L. B.; Eichhorn, S. J.; Kao, C.-C.; Young, R. J. *ACS Appl. Mater. Interfaces* **2011**, *3*, 433–440.
(30) Arlt, C.; Riedel, U.; Wulz, H. G. . In *Proceedings of the 27th Congress of the International Council of the Aeronautical Sciences*; Nice, France, Sept 19−24, 2010; International Council of the Aeronautical Sciences: Bonn, Germany, 2010; 8.4.4.
(31) Qian, H.; Greenhalgh, E. S.; Shaffer, M. S. P.; Bismarck, A. *J. Mater. Chem.* **2010**, *20*, 4751–4762.
(32) Liu, L.; Wagner, H. D. *Compos. Sci. Technol.* **2005**, *65*, 1861–1868.
(33) Ci, L.; Bai, J. *Compos. Sci. Technol.* **2006**, *66*, 599–603.
(34) Velmurugan, R.; Mohan, T. P. *J. Mater. Sci.* **2004**, *39*, 7333–7339.
(35) Marouf, B. T.; Bagheri, R.; Pearson, R. A. *J. Mater. Sci.* **2008**, *43*, 6992–6997.
(36) Tang, Q.-Y.; Chan, Y.-C.; Wong, N.-B.; Cheung, R. *Polym. Int.* **2010**, *59*, 1240–1245.